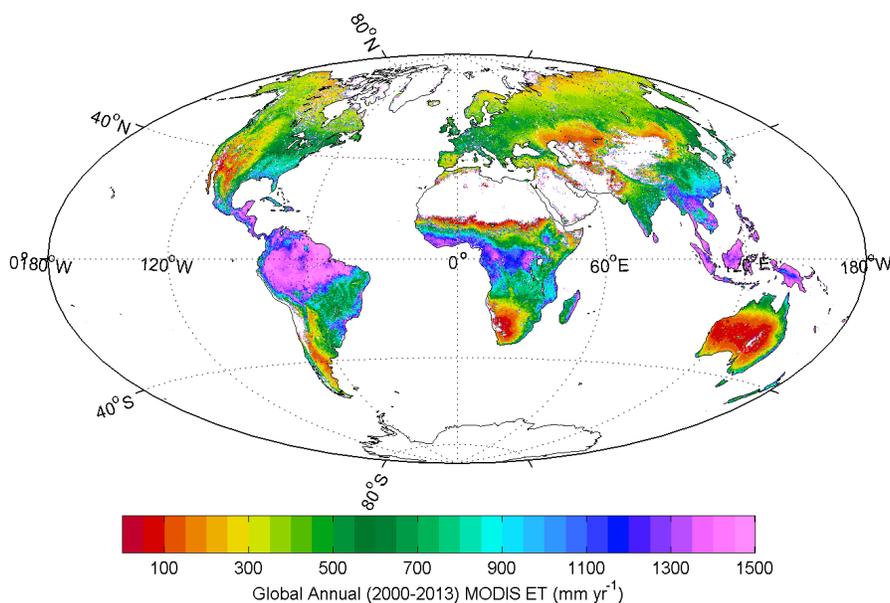# User's Guide
# MODIS Global Terrestrial Evapotranspiration (ET) Product (MOD16A2/A3 and Year-end Gap-filled MOD16A2GF/A3GF) NASA Earth Observing System MODIS Land Algorithm (For Collection 6.1)

**Steven W. Running**
**Qiaozhen Mu**
**Maosheng Zhao**
**Alvaro Moreno**

The C61 MOD/MYD16 product is identical in format to the C6 product. This (C61) reprocessing does not contain any change to the science algorithm used to make this product. Any improvement or change in the C61 product compared to the product from the prior major collection reprocessing (C6) is from changes and enhancements to the calibration approach used in generation of the Terra and Aqua MODIS L1B products and changes to the polarization correction used in this collection reprocessing. For further details on C61 calibration changes and other changes user is encouraged to refer to the Collection 6.1 specific changes that have been summarized here: https://landweb.modaps.eosdis.nasa.gov/QA_WWW/forPage/MODIS_C61_Land_Proposed_Changes.pdf



Global Annual (2000-2013) MODIS ET (mm yr$^{-1}$)

**Version 1.1**
**Mar. 11th, 2021**

**Table of Contents**

## Synopsis

The guide provides a description of the Collection6.1 (C6.1 hereafter) NASA's MODIS terrestrial ecosystem Evapotranspiration (ET), latent heat flux (LE), Potential ET (PET), and Potential LE (PLE) data products at 500m spatial resolution: 8-day MOD16A2 and annual MOD16A3 and their year-end gap-filled data products (MOD16A2GF/A3GF). The global MOD16 data products cover the 109.03 Million km2 global vegetated land areas and designed for the MODIS sensor aboard the Aqua and Terra platforms, beginning in 2000 and continuing to the present. The MOD16 algorithm is based on the logic of the Penman-Monteith equation which uses daily meteorological reanalysis data and 8-day remotely sensed vegetation property dynamics from MODIS as inputs. The data products are archived at a NASA DAAC (Distributed Active Archive Center). This document is intended to provide both a broad overview and sufficient detail to allow for the successful use of the data in research and applications.

Please note the "MOD" prefix should be considered as referring to data sets derived from MODIS onboard either TERRA or Aqua satellite. ***That is, "MOD" in this document can also be treated as "MYD" derived from MODIS on Aqua.***

## 1. The Algorithm, Background and Overview

Calculation of ET is typically based on the conservation of either energy or mass, or both. Computing ET is a combination of two complicated major issues: (1) estimating the stomatal conductance to derive transpiration from plant surfaces; and (2) estimating evaporation from the ground surface. The MOD16 ET algorithm runs at daily basis and temporally, daily ET is the sum of ET from daytime and night. Vertically, ET is the sum of water vapor fluxes from soil evaporation, wet canopy evaporation and plant transpiration at dry canopy surface. Remote sensing has long been recognized as the most feasible means to provide spatially distributed regional ET information on land surfaces. Remotely sensed data, especially those from polar-orbiting satellites, provide temporally and spatially continuous information over vegetated surfaces useful for regional measurement and monitoring of surface biophysical variables affecting ET, including albedo, biome type and leaf area index (LAI) (Los et al., 2000).

### 1.1. Energy Partitioning Logic

Energy partitioning at the surface of the earth is governed by the following three coupled equations:

$$H = \rho\, C_p \frac{T_s - T_a}{r_a} \tag{1}$$

$$\lambda E = \frac{\rho\, C_p (e_{sat} - e)}{\lambda\, (r_a + r_s)} \tag{2}$$

$$A' = R_{net} - \Delta S - G = H + \lambda E \tag{3}$$

where $H$, $\lambda E$ and $A'$ are the fluxes of sensible heat, latent heat and available energy for $H$ and $\lambda E$;

$R_{net}$ is net radiation, $G$ is soil heat flux; $\Delta S$ is the heat storage flux. $\lambda$ is the latent heat of vaporization. $\rho$ is air density, and $C_P$ is the specific heat capacity of air; $T_s$, $T_a$ are the aerodynamic surface and air temperatures; $r_a$ is the aerodynamic resistance; $e_{sat}$, $e$ are the water vapour pressure at the evaporating surface and in the air; $r_s$ is the surface resistance to evapotranspiration, which is an effective resistance to evaporation from land surface and transpiration from the plant canopy. The psychrometric constant $\gamma$ is given by

$$\gamma = \frac{C_p \, P_a \, M_a}{\lambda \, M_w} \tag{4}$$

where $M_a$ and $M_w$ are the molecular masses of dry air and wet air respectively and $P_a$ the atmospheric pressure.

## 1.2. Penman-Monteith Logic

Developing a robust algorithm to estimate global evapotranspiration is a significant challenge. Traditional energy balance models of ET require explicit characterization of numerous physical parameters, many of which are difficult to determine globally. For these models, thermal remote sensing data (e.g., land surface temperature, LST) are the most important inputs. However, using the 8-day composite MODIS LST (the average LST of all cloud-free data in the compositing window) (Wan et al., 2002) and daily meteorological data recorded at the flux tower, Cleugh et al. (2007) demonstrate that the results from thermal models are unreliable at two Australian sites (Virginia Park, a wet/dry tropical savanna located in northern Queensland and Tumbarumba, a cool temperate, broadleaved forest in south east New South Wales). Using a combination of remote sensing and global meteorological data, we have adapted the Cleugh et al. (2007) algorithm, which is based on the Penman–Monteith method and calculates both canopy conductance and ET. Monteith (1965) eliminated surface temperature from Equations (1) – (3) to give:

$$\lambda E = \frac{s \, A' + \rho \, C_p \frac{(e_{sat} - e)}{r_a}}{s + \gamma \left(1 + \frac{r_s}{r_a}\right)} = \frac{s \, A' + \rho \, C_p \frac{VPD}{r_a}}{s + \gamma \left(1 + \frac{r_s}{r_a}\right)} \tag{5}$$

where $s = d(e_{sat})/dT$, the slope of the curve relating saturated water vapor pressure ($e_{sat}$) to temperature; $A'$ is available energy partitioned between sensible heat and latent heat fluxes on land surface. $VPD = e_{sat} - e$ is the air vapor pressure deficit. All inputs have been previously defined except for surface resistance $r_s$, which is an effective resistance accounting for evaporation from the soil surface and transpiration from the plant canopy.

Despite its theoretical appeal, the routine implementation of the P-M equation is often hindered by requiring meteorological forcing data ($A'$, $T_a$ and $VPD$) and the aerodynamic and surface resistances ($r_a$ and $r_s$). Radiation and soil heat flux measurements are needed to determine $A'$; air temperature and humidity to calculate $VPD$; and wind speed and surface roughness parameters to determine $r_a$. Multi-temporal implementation of the P-M model at regional scales requires routine surface meteorological observations of air temperature, humidity, solar radiation and wind speed. Models for estimating maximum stomatal conductance including the effect of

limited soil water availability and stomatal physiology requires either a fully coupled biophysical model such as that by Tuzet et al. (2003) or resorting to the empirical discount functions of Jarvis (1976), which must be calibrated. Determining a surface resistance for partial canopy cover is even more challenging with various dual source models proposed (e.g. Shuttleworth and Wallace, 1985) to account for the presence of plants and soil.

## 2. The MOD16A2/MOD16A3 algorithm logic

MOD16 ET algorithm is based on the Penman-Monteith equation (Monteith, 1965) as in equation 5.  Figure 2 shows the logic behind the improved MOD16 ET Algorithm for calculating daily MOD16 ET algorithm.
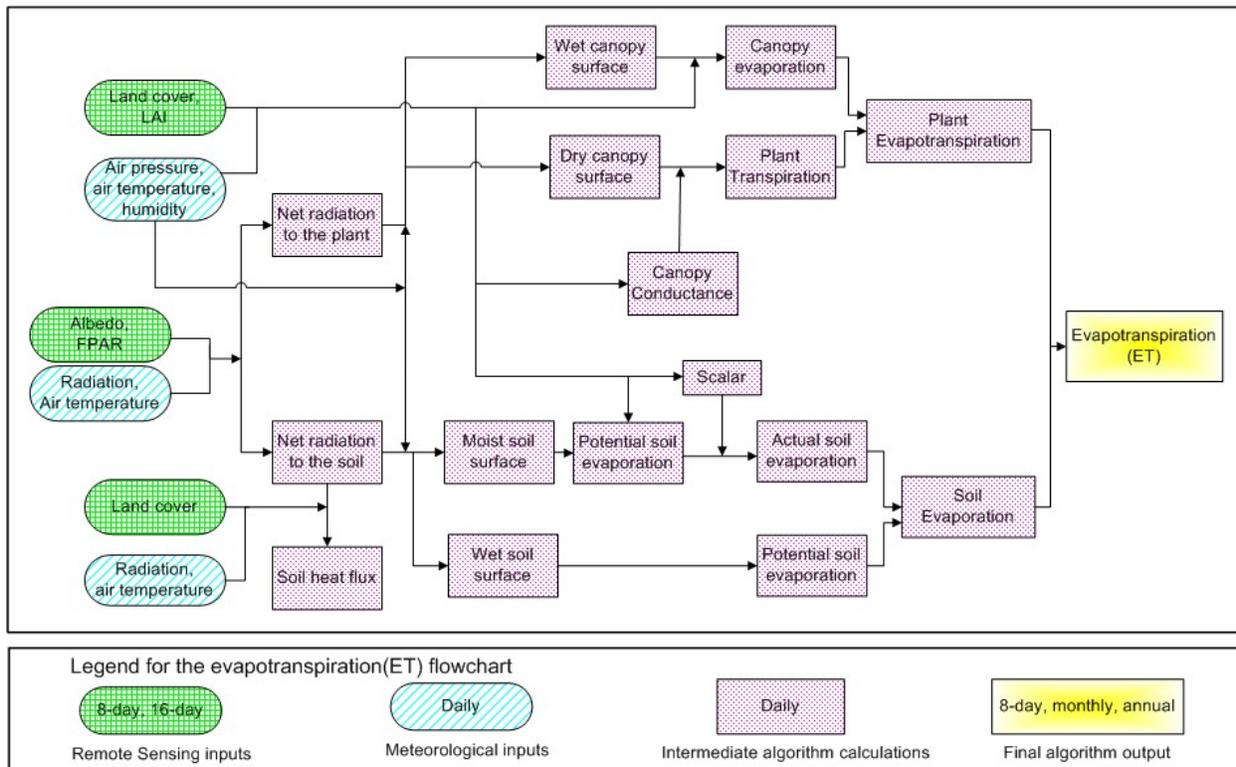


***Figure 2.*** Flowchart of the improved MOD16 ET algorithm.  LAI: leaf area index; FPAR: Fraction of Photosynthetically Active Radiation. Net radiation calculation and the use of FPAR are detailed in section 2.2.

### 2.1. Daytime and Nighttime ET

Daily ET should be the sum of daytime and nighttime ET. To separate daytime and nighttime ET, we first obtain their air temperature which will be used in the following sections to calculate the two ET components. To get nighttime average air temperature $(T_{night})$, we assume that daily average air temperature $(T_{avg})$ is the average of daytime air temperature $(T_{day})$ and $T_{night}$, and $T_{day}$ is the average of air temperature when downward solar radiation is above 0. Thus,

$$T_{night} = 2 * T_{avg} - T_{day} \tag{6}$$

The net incoming solar radiation at night is assumed to be zero. Based on the optimization theory, stomata will close at night to prevent water loss when there is no opportunity for carbon gain (Dawson et al., 2007). In the improved ET algorithm, at night, the stomata are assumed to close completely and the plant transpiration through stomata is zero, except for the transpiration through leaf boundary-layer and leaf cuticles (more details in section 2.5). Both nighttime and daytime use the same ET algorithm except that different values at daytime and nighttime are used for the same variable.

## 2.2. Soil Heat Flux

In MOD16 ET algorithm, the net incoming radiation to the land surface ($R_{net}$) is calculated as the equations 7 and 8 (Cleugh et al., 2007).

$$R_{net} = (1 - a)R_{s\downarrow} + \sigma (\varepsilon_a - \varepsilon_s)(273.15 + T)^4 \tag{7}$$

$$\varepsilon_a = 1 - 0.26 \, e^{(-7.77 \cdot 10^{-4} T^2)}$$

$$\varepsilon_s = 0.97$$

where α is MODIS albedo, $R_{s\downarrow}$ is the downward shortwave radiation, $\varepsilon_s$ is surface emissivity, $\varepsilon_a$ is atmospheric emissivity, and $T$ is air temperature in °C. At daytime, if $R_{net}$ is less than zero, $R_{net}$ is set to be zero; at nighttime, if $R_{net}$ is less than -0.5 times of daytime $R_{net}$, nighttime $R_{net}$ is set as -0.5 multiplying daytime $R_{net}$. There is no soil heat flux (G) interaction between the soil and atmosphere if the ground is 100% covered with vegetation. Energy received by soil is the difference between the radiation partitioned on the soil surface and soil heat flux (G).

$$A = R_{net} \tag{8}$$

$$A_c = F_c \, A$$

$$A_{soil} = (1 - F_c) \, A - G$$

where $A$ is available energy partitioned between sensible heat, latent heat and soil heat fluxes on land surface; $R_{net}$ is the net incoming radiation received by land surface; $A_c$ is the part of $A$ allocated to the canopy and $A_{soil}$ is the part of $A$ partitioned on the soil surface. Net radiation is partitioned between the canopy and soil surface based on vegetation cover fraction ($F_C$), in order to reduce numbers of inputs from MODIS datasets and to simplify the algorithm, we use 8-day 0.5 km$^2$ MOD15A2H FPAR (the Fraction of Absorbed Photosynthetically Active Radiation) as a surrogate of vegetation cover fraction (Los et al., 2000), $F_C = FPAR$.

At the extremely hot or cold places or when the difference between daytime and nighttime temperature is low (<5°C), there is no soil heat flux. The soil heat flux is estimated as:

$$G_{soil} = \begin{cases} 4.73\,T_i - 20.87 & T_{min\,close} \leq Tann_{avg} < 25°C, T_{day} - T_{night} \geq 5°C \\ 0 & Tann_{avg} \geq 25°C \text{ or } Tann_{avg} < T_{min\,close} \text{ or } T_{day} - T_{night} \geq 5°C \\ 0.39 A_i & abs(G_{soil}) > 0.39\,abs(A_i) \end{cases}$$

$$G = G_{soil}(1 - F_c) \tag{9}$$

where $G_{soil}$ stands for the soil heat flux when $F_C = 0$; $T_i$ means daytime or nighttime average temperature in °C; $Tann_{avg}$ is annual average daily temperature, and $T_{min\,close}$ is the threshold value below which the stomata will close completely and halt plant transpiration (Table 3.2; Running et al., 2004; Mu et al., 2007; Mu et al., 2011). At daytime, $G_{soil\,day} = 0.0$ if $A_{day} - G_{soil\,day} < 0.0$; at nighttime, $G_{soil\,night} = A_{night} + 0.5 A_{day}$ if $A_{day} > 0.0$ and $A_{night} - G_{night} < -0.5\,A_{day}$.

## 2.3. Wet Surface Fraction

In the MOD16 algorithm, ET is the sum of water lost to the atmosphere from the soil surface through evaporation, canopy evaporation from the water intercepted by the canopy, and transpiration from plant tissues (Fig. 2). The land surface is covered by the plant and the bare soil surface, and percentage of the two components is determined by $F_C$. Both the canopy and the soil surface are partly covered by water under certain conditions. The water cover fraction ($F_{wet}$) is taken from the Fisher et al. (2008) ET model, modified to be constrained to zero when relative humidity (RH) is less than 70%:

$$F_{wet} = \begin{cases} 0 & RH < 70\% \\ RH^4 & 70\% \leq RH \leq 100\% \end{cases} \tag{10}$$

where *RH* is relative humidity (Fisher et al, 2008). When *RH* is less than 70%, 0% of the surface is covered by water. For the wet canopy and wet soil surface, the water evaporation is calculated as the potential evaporation as described in the next sections (2.4 and 2.6).

## 2.4. Evaporation from Wet Canopy Surface

Evaporation of precipitation intercepted by the canopy accounts for a substantial amount of upward water flux in ecosystems with high LAI. When the vegetation is covered with water (i.e., $F_{wet}$ is not zero), water evaporation from the wet canopy surface will occur. ET from the vegetation consists of the evaporation from the wet canopy surface and transpiration from plant tissue, whose rates are regulated by aerodynamics resistance and surface resistance.

The aerodynamic resistance (*rhrc*, s m⁻¹) and wet canopy resistance (*rvc*, s m⁻¹) to evaporated water on the wet canopy surface are calculated as

$$rhc = \frac{1}{gl_{sh} LAI\, F_{wet}} \tag{11}$$

$$rrc = \frac{\rho \, C_p}{4 \, \sigma \, (T_i + 273.15)^3}$$

$$rhrc = \frac{rhc \, rrh}{rhc + rrh}$$

$$rvc = \frac{1}{gl_{e \, wv} LAI \, F_{wet}}$$

where *rhc* (s m$^{-1}$) is the wet canopy resistance to sensible heat, *rrc* (s m$^{-1}$) is the resistance to radiative heat transfer through air; $gl_{sh}$ (s m$^{-1}$) is leaf conductance to sensible heat per unit LAI, $gl_{e \, wv}$ (m s$^{-1}$) is leaf conductance to evaporated water vapor per unit LAI, σ (W m$^{-2}$ K$^{-4}$) is Stefan-Boltzmann constant.

Following Biome-BGC model (Thornton, 1998) with revision to account for wet canopy, the evaporation on wet canopy surface is calculated as

$$\lambda E_{wet \, c} = \frac{\left( s \, A_c + \rho \, C_p F_c \dfrac{(e_{sat} - e)}{rhrc} \right) F_{wet}}{s + \dfrac{P_a \, C_p \, rvc}{\lambda \, \varepsilon \, rhrc}} \tag{12}$$

where the resistance to latent heat transfer (*rvc*) is the sum of aerodynamic resistance (*rhrc*) and surface resistance (*r$_s$*) in equation 5.

## 2.5. Plant Transpiration

### 2.5.1. Surface Conductance to Transpiration

Plant transpiration occurs not only during daytime but also at nighttime. For many plant species, stomatal conductance($G_s^1$) decreases as vapor pressure deficit (VPD) increases, and stomatal conductance is further limited by both low and high temperatures (Jarvis, 1976; Sandford and Javis, 1986; Kawamitsu et al., 1993; Schulze et al., 1994; Leuning, 1995; Marsden et al., 1996; Dang et al., 1997; Oren et al., 1999; Xu et al., 2003; Misson et al., 2004). Because high temperatures are often accompanied by high VPDs, we have only added constraints on stomatal conductance for VPD and minimum air temperature ignoring constraints resulting from high temperature. Based on the optimization theory, stomata will close at night to prevent water loss when there is no opportunity for carbon gain (Dawson et al., 2007).

$$G_{s \, i}^1 = \begin{cases} C_L \, m(Tmin) \, m(VPD) \, r_{corr} & i = daytime \\ 0 & i = nighttime \end{cases} \tag{13}$$

The components of each terms in the above equation is calculated as below

$$r_{corr} = \cfrac{1}{\cfrac{101300}{P_a}\left(\cfrac{T_i + 273.15}{293.15}\right)^{1.75}}$$

$$m(T_{min}) = \begin{cases} 1 & T_{min} \geq T_{min\,open} \\ \cfrac{T_{min} - T_{min\,close}}{T_{min\,open} - T_{min\,close}} & T_{min\,close} < T_{min} < T_{min\,open} \\ 0 & T_{min} \leq T_{min\,close} \end{cases}$$

$$m(VPD) = \begin{cases} 1 & VPD \leq VPD_{open} \\ \cfrac{VPD_{close} - VPD}{VPD_{close} - VPD_{open}} & VPD_{open} < VPD < VPD_{close} \\ 0 & VPD \geq VPD_{close} \end{cases}$$

where $C_L$ is the mean potential stomatal conductance per unit leaf area, $C_L$ is set differently for different biomes as shown in Table 3.2 (Kelliher et al., 1995; Schulze et al., 1994; White et al., 2000), $m(T_{min})$ is a multiplier that limits potential stomatal conductance by minimum air temperatures ($T_{min}$), and $m(VPD)$ is a multiplier used to reduce the potential stomatal conductance when $VPD$ (difference between $e_{sat}$ and $e$) is high enough to reduce canopy conductance. Sub index *close* indicates nearly complete inhibition (full stomatal closure) due to low $T_{min}$ and high $VPD$, and *open* indicates no inhibition to transpiration (Table 3.2). When $T_{min}$ is lower than the threshold value $T_{min\,close}$, or $VPD$ is higher than the threshold $VPD_{close}$, the strong stresses from temperature or water availability will cause stomata to close completely, halting plant transpiration. On the other hand, when $T_{min}$ is higher than $T_{min\,open}$, and $VPD$ is lower than $VPD_{open}$, there will be no temperature or water stress on transpiration. For $T_{min}$ and $VPD$ falling into the range of the upper and low limits, the corresponding multiplier will be within 0.0 to 1.0, implying a partial stomatal closure. The multipliers range linearly from 0 (total inhibition, limiting $r_s$) to 1 (no inhibition) for the range of biomes are listed in a Biome Properties Look-Up Table (BPLUT) (Table 3.2).

The reason we use the correction function $r_{corr}$ for calculation of stomatal conductance is that the conductance through air varies with the air temperature and pressure. The prescribed values are assumed to be given for standard conditions of 20°C and 101300 Pa. Based on the prescribed daily air temperature (converted to Kelvins) and an air pressure estimated from a prescribed elevation, the prescribed standard conductance is converted to actual conductance for the day according to Jones (1992) and Thornton (1998). $P_a$ is calculated as a function of the elevation (Thornton, 1998).

$$t_1 = 1 - \frac{LR_{STD}\,Elev}{T_{STD}}$$
$$t_2 = \frac{G_{STD}}{LR_{STD}\cfrac{RR}{MA}} \tag{14}$$
$$P_a = P_{STD}\,t_1^{t_2}$$

where $LR_{STD}$, $T_{STD}$, $G_{STD}$, $RR$, $MA$ and $P_{STD}$ are constant values as listed in Table 2.1 $LR_{STD}$ (K m$^{-1}$) is standard temperature lapse rate; $T_{STD}$ (K) is standard temperature at 0.0 m elevation; $G_{STD}$ (m s$^{-2}$) is standard gravitational acceleration; $RR$ (m$^3$ P$_a$ mol$^{-1}$ K$^{-1}$) is gas law constant; $MA$ (kg mol$^{-1}$) is molecular weight of air and $P_{STD}$ (Pa) is standard pressure at 0 m elevation.

**Table 2.1** Other parameter values as used in the improved ET algorithm

| $LR_{STD}$ (K m$^{-1}$) | $T_{STD}$ (K) | $G_{STD}$ (m s$^{-2}$) | $RR$ (m$^3$ Pa mol$^{-1}$ K$^{-1}$) | $MA$ (kg mol$^{-1}$) | $P_{STD}$ (Pa) |
|---|---|---|---|---|---|
| 0.0065 | 288.15 | 9.80665 | 8.3143 | 28.9644e-3 | 101325.0 |

Canopy conductance ($C_c$) to transpired water vapor per unit LAI is derived from stomatal and cuticular conductance in parallel with each other, and both in series with leaf boundary layer conductance (Thornton, 1998; Running & Kimball, 2005). In the case of plant transpiration, surface conductance is equivalent to the canopy conductance ($C_C$), and hence surface resistance ($R_s$) is the inverse of canopy conductance ($C_C$).

$$C_{ci} = \begin{cases} \dfrac{G_s^2(G_{si}^1 + G_{CU})}{G_{si}^1 + G_s^2 + G_{CU}} \, LAI \, (1 - F_{wet}) & (LAI > 0, (1 - F_{wet}) > 0) \\ 0 & (LAI = 0, (1 - F_{wet}) = 0) \end{cases}$$

(15)

$$G_{cu} = g_{cu} \, r_{corr}$$

$$G_s^2 = gl_{sh}$$

$$r_{si} = \frac{1}{C_{ci}}$$

where the subscript $i$ means the variable value at daytime and nighttime; $G_{CU}$ is leaf cuticular conductance; $G_s^2$ is leaf boundary-layer conductance; $g_{cu}$ is cuticular conductance per unit LAI, set as a constant value of 0.00001 (m s$^{-1}$) for all biomes; $gl_{sh}$ is leaf conductance to sensible heat per unit LAI, which is a constant value for each given biome (Table 3.2).

### 2.5.2. Aerodynamic Resistance

The transfer of heat and water vapor from the dry canopy surface into the air above the canopy is determined by the aerodynamic resistance ($r_a$). $r_a$ is calculated as a parallel resistance to convective ($rh$) and radiative ($rr$) heat transfer following Biome-BGC model (Thornton, 1998).

$$r_a = \frac{rh \, rr}{rh + rr}$$

$$rh = \frac{1}{gl_{bl}}$$

(16)

$$rr = \frac{\rho \, C_p}{4 \, \sigma \, (T_i + 273.15)^3}$$

where $gl_{bl}$ (m s$^{-1}$) is leaf-scale boundary layer conductance, whose value is equal to leaf conductance to sensible heat per unit LAI ($gl_{sh}$ (m s$^{-1}$) as in section 2.4), and σ (W m$^{-2}$ K$^{-4}$) is

Stefan-Boltzmann constant.

### 2.5.3. *Plant Transpiration*

Finally, the plant transpiration ($AE_{trans}$) is calculated as

$$\lambda E_{trans} = \frac{\left(s\, A_c + \rho\, C_p F_c \dfrac{(e_{sat} - e)}{r_a}\right)(1 - F_{wet})}{s + \gamma\left(1 + \dfrac{r_s}{r_a}\right)} \tag{17}$$

where $r_a$ is the aerodynamic resistance calculated from equation 5.

$$\lambda E_{pot\ trans} = \frac{\alpha\, s\, A_c\, (1 - F_{wet})}{s + \gamma} \tag{18}$$

with $\alpha = 1.26$.

### 2.6. Evaporation from Soil Surface

The soil surface is divided into the saturated surface covered with water and the moist surface by $F_{wet}$. The soil evaporation includes the potential evaporation from the saturated soil surface and evaporation from the moist soil surface. The total aerodynamic resistance to vapor transport ($r_{tot}$) is the sum of surface resistance ($r_s$) and the aerodynamic resistance for vapor transport ($r_v$) such that $r_{tot\ =} r_v + r_s$ (van de Griend & Owe, 1994; Mu et al., 2007). We assume that $r_v$ ($s\ m^{-1}$) is equal to the aerodynamic resistance ($r_a$: $s\ m^{-1}$) in Equation 5 since the values of $r_v$ and $ra$ are usually very close (van de Griend & Owe, 1994). In the MOD16 ET algorithm, the $rhs$ is assumed to be equal to boundary layer resistance, which is calculated in the same way as total aerodynamic resistance ($r_{tot}$) (Thornton, 1998) only that, $r_{totc}$ is not a constant. For a given biome type, there is a maximum ($rbl_{max}$) and a minimum value ($rbl_{min}$) for $r_{totc}$, and $r_{totc}$ is a function of VPD.

$$r_{tot} = r_{totc}\, r_{corr} \tag{19}$$

$$r_{totc} = \begin{cases} rbl_{max} & VPD \leq VPD_{open} \\ rbl_{max} - \dfrac{(rbl_{max} - rbl_{min})(VPD_{close} - VPD)}{VPD_{close} - VPD_{open}} & VPD_{open} < VPD < VPD_{close} \\ rbl_{min} & VPD \geq VPD_{close} \end{cases}$$

where $r_{corr}$ is the correction for atmospheric temperature and pressure (equation 13) above mentioned. The values of $rbl_{max}$ and $rbl_{min}$, $VPD_{open}$ (when there is no water stress on transpiration) and $VPD_{close}$ (when water stress causes stomata to close almost completely, halting plant transpiration) are parameterized differently for different biomes and are listed in Table 3.2.

The aerodynamic resistance at the soil surface ($r_{as}$) is parallel to both the resistance to convective heat transfer ($rhs$: $s\ m^{-1}$) and the resistance to radiative heat transfer ($r_{rs}$: $s\ m^{-1}$) (Choudhury and DiGirolamo, 1998), such that

$$r_{as} = \frac{r_{hs}\, r_{rs}}{r_{hs} + r_{rs}}$$

$$r_{hs} = r_{tot} \qquad\qquad\qquad\qquad\qquad\qquad\qquad\qquad\qquad\qquad\qquad (20)$$

$$r_{rs} = \frac{\rho\, C_p}{4\, \sigma\, (T_i + 273.15)^3}$$

The actual soil evaporation ($\lambda E_{SOIL}$) is calculated in equation 21 using potential soil evaporation ($\lambda E_{SOIL\,POT}$) and soil moisture constraint function in the Fisher et al. (2008) ET model. This function is based on the complementary hypothesis (Bouchet, 1963), which defines land-atmosphere interactions from air *VPD* and relative humidity (*RH*, %).

$$\lambda E_{wet\,soil} = \frac{\left(s\, A_{soil} + \rho\, C_p(1 - F_c)\dfrac{VPD}{r_{as}}\right) F_{wet}}{s + \gamma\dfrac{r_{tot}}{r_{as}}}$$

$$\lambda E_{soil_{pot}} = \frac{\left(s\, A_{soil} + \rho\, C_p(1 - F_c)\dfrac{VPD}{r_{as}}\right)(1 - F_{wet})}{s + \gamma\dfrac{r_{tot}}{r_{as}}} \qquad\qquad (21)$$

$$\lambda E_{soil} = \lambda E_{wet\,soil} + \lambda E_{soil_{pot}} \left(\frac{RH}{100}\right)^{\frac{VPD}{\beta}}$$

with β = 250.

## 2.7. Total Daily Evapotranspiration

The total daily ET is the sum of evaporation from the wet canopy surface, the transpiration from the dry canopy surface and the evaporation from the soil surface. The total daily ET and potential ET$(\lambda E_{POT})$ are calculated as in equation 22.

$$\lambda E = \lambda E_{wet\,c} + \lambda E_{trans} + \lambda E_{soil} \qquad\qquad\qquad\qquad\qquad (22)$$

$$\lambda E_{pot} = \lambda E_{wet\,c} + \lambda E_{pot\,trans} + \lambda E_{wet\,soil} + \lambda E_{soil\,pot}$$

Combination of ET with the potential ET can determine environmental water stress and detect the intensity of drought.

## 2.8. Updates after Publication of RSE Paper by Mu et al. (2011)

The MOD16 products are generated based on the MOD16 algorithm in Mu et al.'s 2011 RSE paper. Since the publication, Dr. Mu have updated the product to fix some issues and these updates have been implemented in the operational code.

1. Issue of negative ET and PET values for some 8-day and monthly data.

In the previous product, we allowed the net incoming daytime radiation to be negative. Only MERRA daytime downward solar radiation, daytime actual vapor pressure, daytime

temperature, daily average and minimum temperatures are used as meteorological inputs. The outgoing and incoming longwave radiation is calculated as in Mu et al.'s 2011 RSE paper.    In the updated product, the nighttime actual vapor pressure, nighttime temperature, outgoing and incoming longwave radiation are from MERRA directly. If daytime $R_{net} < 0$; daytime $R_{net} = 0$.

In the MOD16 ET algorithm, when we calculated the soil heat flux, we didn't constrain the soil heat flux. The net radiation to the bare ground is difference between the fraction of the net incoming radiation reaching to the ground surface (Rground) and the soil heat flux (G). In certain cases, G is higher than Rground, resulting in negative soil evaporation.    In the updated product, We set limit to G.    For daytime $R_{net}$ and $G$:

$if\ (R_{net} - G) < 0;\ \ \ G = R_{net}$

Whereas for nighttime $R_{net}$ and $G$:

$if\ (R_{net} - G) < -0.5 * daytime\ R_{net};\ \ \ G = R_{net} + 0.5 * daytime\ R_{net}$

2. Issue of no valid MODIS surface albedo values throughout the year for vegetated pixels due to high frequency of cloudiness.

In the improved MOD16. For example, no single valid MODIS albedo can be found throughout an entire year over rainforests of west Africa due to severe and constant cloudiness. In the update version, we specify an albedo value of 0.4 for the pixels, a typical value for nearby rainforests with valid albedo values.

## 3.  Operational Details of MOD16 and Primary Uncertainties in the MOD16 Logic

A number of issues are important in implementing this algorithm. This section discusses some of the assumptions and special issues involved in development of the input variables, and their influence on the final ET estimates.

### 3.1. Dependence on MODIS Land Cover Classification MCDLCHKM
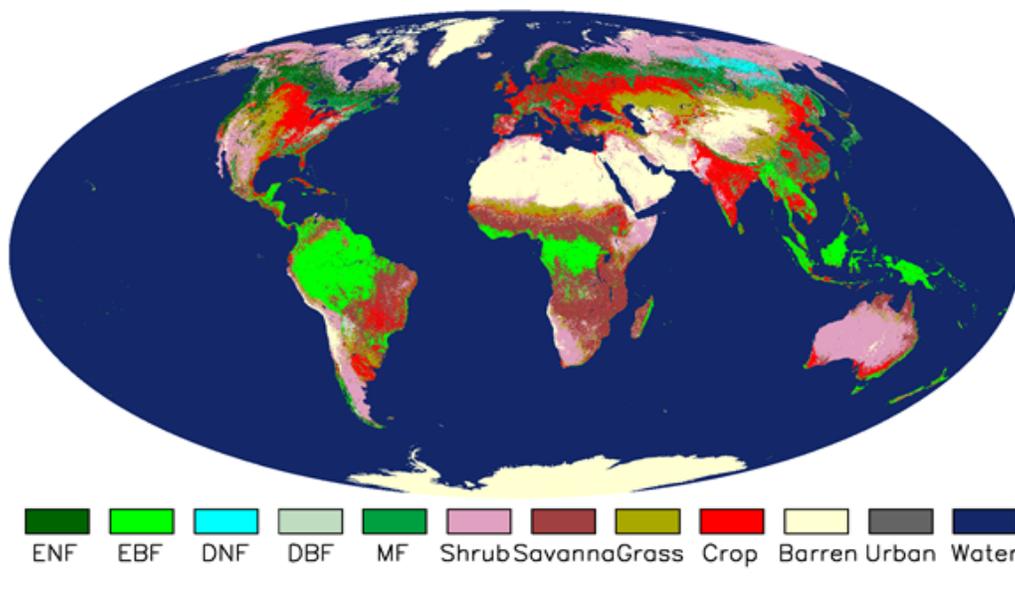


***Figure 3.1.*** *Collection5 1-km MODIS ET used land cover type 2 in 1-km Collection4 MOD12Q1 dataset. Whereas Collection6 operational 500-m MODIS ET is using land cover type 1 in*

*Collection5.1 500-m MCDLCHKM which is a 3-year smoothed MODIS land cover data set. This figures shows land cover types from the Collection4 MOD12Q1 dataset: Evergreen Needleleaf Forest (ENF), Evergreen Broadleaf Forest (EBF), Deciduous Needleleaf Forest (DNF), Deciduous Broadleaf Forest (DBF), Mixed forests (MF), Closed Shrublands (CShrub), Open Shrublands (OShrub), Woody Savannas (WSavanna), Savannas (Savanna), grassland (Grass), and Croplands (Crop). Note that in this figure, we combined CShrub and OShrub into Shrub, and WSavanna and Savannas into Savanna. Globally, Collection5.1 500-m MCDLCHKM has a similar spatial pattern to this image.*

One of the first MODIS products used in the MOD16 algorithm is the Land Cover Product. For the previous Collection5 1-km MODIS ET, the 1-km land cover type 2 in a frozen version of the Collection4 MOD12Q1 was used. However, for the operational Collection 6 500-m MODIS ET, a 3-year smoothed land cover data set, land cover type 1 in the Collection5.1 500-m MCDLCHKM, is being used. The importance of this product cannot be overstated as the MOD16 algorithm relies heavily on land cover type through use of the BPLUT. The land cover type 1 created by 500-m MCDLCHKM is a 17-class IGBP (International Geosphere-Biosphere Programme) land cover classification map (Running et al. 1994, Belward et al. 1999, Friedl et al. 2010) (Table 3.1). Figure 3.1 shows the Collection4 1-km MOD12Q1 dataset used by the Collection5 MODIS ET. Globally, Collection5.1 500-m MCDLCHKM has a very similar spatial pattern to this image though it may have a different land cover type for a given pixel.

### 3.1.1. The BPLUT and constant biome properties

**Table 3.1**. *The land cover types used in the MOD16 Algorithm.*

| Land Cover Type 1 in 500-m MCDLCHKM | |
|---|---|
| **Class Value** | **Class Description** |
| 0 | Water |
| 1 | Evergreen Needleleaf Forest |
| 2 | Evergreen Broadleaf Forest |
| 3 | Deciduous Needleleaf Forest |
| 4 | Deciduous Broadleaf Forest |
| 5 | Mixed Forest |
| 6 | Closed Shrubland |
| 7 | Open Shrubland |
| 8 | Woody Savanna |
| 9 | Savanna |
| 10 | Grassland |
| 12 | Cropland |
| 13 | Urban or Built-Up |
| 16 | Barren or Sparsely Vegetated |
| 254 | Unclassified |
| 255 | Missing Data |

Arguably, the most significant assumption made in the MOD16 logic is that biome-specific physiological parameters do not vary with space or time. These parameters are outlined in the

BPLUT (Table 3.2) within the MOD16 algorithm. The BPLUT constitutes the physiological framework for controlling simulated ET.  These biome-specific properties are not differentiated for different expressions of a given biome, nor are they varied at any time during the year.  In other words, a semi-desert grassland in Mongolia is treated the same as a tallgrass prairie in the Midwestern United States.  Likewise, a sparsely vegetated boreal evergreen needleleaf forest in Canada is functionally equivalent to its coastal temperate evergreen needleleaf forest counterpart**.**

**Table 3.2.** *Biome-Property-Look-Up-Table (BPLUT) for MODIS ET algorithm with NCEP-DOE reanalysis II and the Collection 6 FPAR/LAI/Albedo as inputs. The full names for land cover classification system in 500-m MCDLCHKM dataset (fieldname: Land_Cover_Type_1) are, Evergreen Needleleaf Forest (ENF), Evergreen Broadleaf Forest (EBF), Deciduous Needleleaf Forest (DNF), Deciduous Broadleaf Forest (DBF), Mixed forests (MF), Closed Shrublands (CShrub), Open Shrublands (OShrub), Woody Savannas (WSavanna), Savannas (Savanna), Grassland (Grass), and Croplands (Crop). Note this table has been updated since publication of RSE paper by Mu et al. (2011), and please refer to section 2.8 for details.*

| VEG_LC | ENF | EBF | DNF | DBF | MF | CShrub | OShrub | WSavanna | Savanna | Grass | Crop |
|--------|-----|-----|-----|-----|----|--------|--------|----------|---------|-------|------|
| $Tmin_{close}$ (C) | -8.00 | -8.00 | -8.00 | -6.00 | -7.00 | -8.00 | -8.00 | -8.00 | -8.00 | -8.00 | -8.00 |
| $Tmin_{open}$ (C) | 8.31 | 9.09 | 10.44 | 9.94 | 9.50 | 8.61 | 8.80 | 11.39 | 11.39 | 12.02 | 12.02 |
| $VPD_{open}$ (Pa) | 650.0 | 1000.0 | 650.0 | 650.0 | 650.0 | 650.0 | 650.0 | 650.0 | 650.0 | 650.0 | 650.0 |
| $VPD_{close}$ (Pa) | 3000.0 | 4000.0 | 3500.0 | 2900.0 | 2900.0 | 4300.0 | 4400.0 | 3500.0 | 3600.0 | 4200.0 | 4500.0 |
| $gl_{sh}$ (m s$^{-1}$) | 0.01 | 0.01 | 0.01 | 0.01 | 0.01 | 0.02 | 0.02 | 0.04 | 0.04 | 0.02 | 0.02 |
| $gl_{e\,wv}$ (m s$^{-1}$) | 0.01 | 0.01 | 0.01 | 0.01 | 0.01 | 0.02 | 0.02 | 0.04 | 0.04 | 0.02 | 0.02 |
| $g_{cu}$ (m s$^{-1}$) | 0.00001 | 0.00001 | 0.00001 | 0.00001 | 0.00001 | 0.00001 | 0.00001 | 0.00001 | 0.00001 | 0.00001 | 0.00001 |
| $C_L$ (m s$^{-1}$) | 0.00240 | 0.00240 | 0.00240 | 0.00240 | 0.00240 | 0.00550 | 0.00550 | 0.00550 | 0.00550 | 0.00550 | 0.00550 |
| $rbl_{min}$ (s m$^{-1}$) | 60.0 | 60.0 | 60.0 | 60.0 | 60.0 | 60.0 | 60.0 | 60.0 | 60.0 | 60.0 | 60.0 |
| $rbl_{max}$ (s m$^{-1}$) | 95.0 | 95.0 | 95.0 | 95.0 | 95.0 | 95.0 | 95.0 | 95.0 | 95.0 | 95.0 | 95.0 |

## 3.2 Leaf area index, fraction of absorbed photosynthetically active radiation and albedo

The FPAR/LAI product is an 8-day composite product. The MOD15 compositing algorithm uses a simple selection rule whereby the maximum FPAR (across the eight days) is chosen for the inclusion as the output pixel. The same day chosen to represent the FPAR measure also contributes the current pixel's LAI value. This means that although ET is calculated daily, the MOD16 algorithm necessarily assumes that leaf area and FPAR do not vary during a given 8-day period. Compositing of LAI and FPAR is required to provide an accurate depiction of global leaf area dynamics with consideration of spectral cloud contamination, particularly in the tropics.

The MCD43A2/A3 albedo products are 16-day moving daily products too. Both Terra and Aqua data are used in the generation of this product, providing the highest probability for quality input data and designating it as an "MCD," meaning "Combined," product. Version-6 MODIS/Terra+Aqua BRDF/Albedo products are Validated Stage 1, indicating that accuracy has been estimated using a small number of independent measurements obtained from selected locations and time periods and ground-truth/field program efforts. Although there may be later improved versions, these data are ready for use in scientific publications.

### 3.2.1. Cloud/Aerosol Screening for Year-end Gap-filled MOD16A2[3]GF

The 8-day MOD15A2H and daily MCD43A3 are still contaminated by clouds and/or aerosols in certain regions and times of year. As a result, in regions with higher frequencies of cloud cover, such as tropical rain forests, values of FPAR/LAI will be greatly reduced and the albedo signal dramatically increased. Previously, gap-filled, or so-called the improved Collection5 (C5 hereafter) MOD16, could only be available from the website of the MOD16's Principal Investigator's lab, the Numerical Terradynamic Simulation Group at the University of Montana (www.ntsg.umt.edu). Now NASA's operational MOD16 data production system is adopting the gap-filling method proposed by Zhao, Mu and their colleagues (Zhao et al., 2005; Mu et al., 2007; Mu et al., 2011) and is implementing it in the Collection6.1 (hereafter C6.1) year-end gap-filled MOD16 operational system. Note that for Collection6 (hereafter C6) gap-filled MOD16, only year-end filling FPAR/LAI is implemented whereas albedo from MCD43A3 has not been filled. From C6.1 near real-time 8-day M*D16A2 is now using the climatology FPAR/LAI and gap-filled albedo of the previous year as backup input to replace the contaminated, resulting in an improved and more useful M*D16A2 for near real-time users. In the below two subsections, we detail the differences in the C6.1 and Gap-filled C6.1 and how the year-end gap-filling method is implemented to generate the higher quality MOD16.

#### 3.2.1.1. Differences between C6.1 and C6 MOD16A2

Cloud-contaminated MODIS inputs can introduce substantial errors or data gaps to the MOD16 data products, and this is the reason that NTSG had decided to improve MOD16 quality through a year-end post-processing, by cleaning these contaminated MODIS inputs (details in section 3.2.1.3; Mu et al., 2007; and Mu et al., 2011). NASA's MODIS Adaptive Processing System (MODAPS) has adopted this same post-processing method to essentially generate the same set of year-end gap-filled MOD16 products that had produced at NTSG for the Collection5 MOD16. These year-end MOD16 products, produced by NASA MODAPS, are referred as MOD16A2GF/MYD16A2GF and MOD16A3GF/MYD16A3GF for the 8-day and Annual Terra and Aqua products respectively, which is detailed in the below section 3.2.1.2.
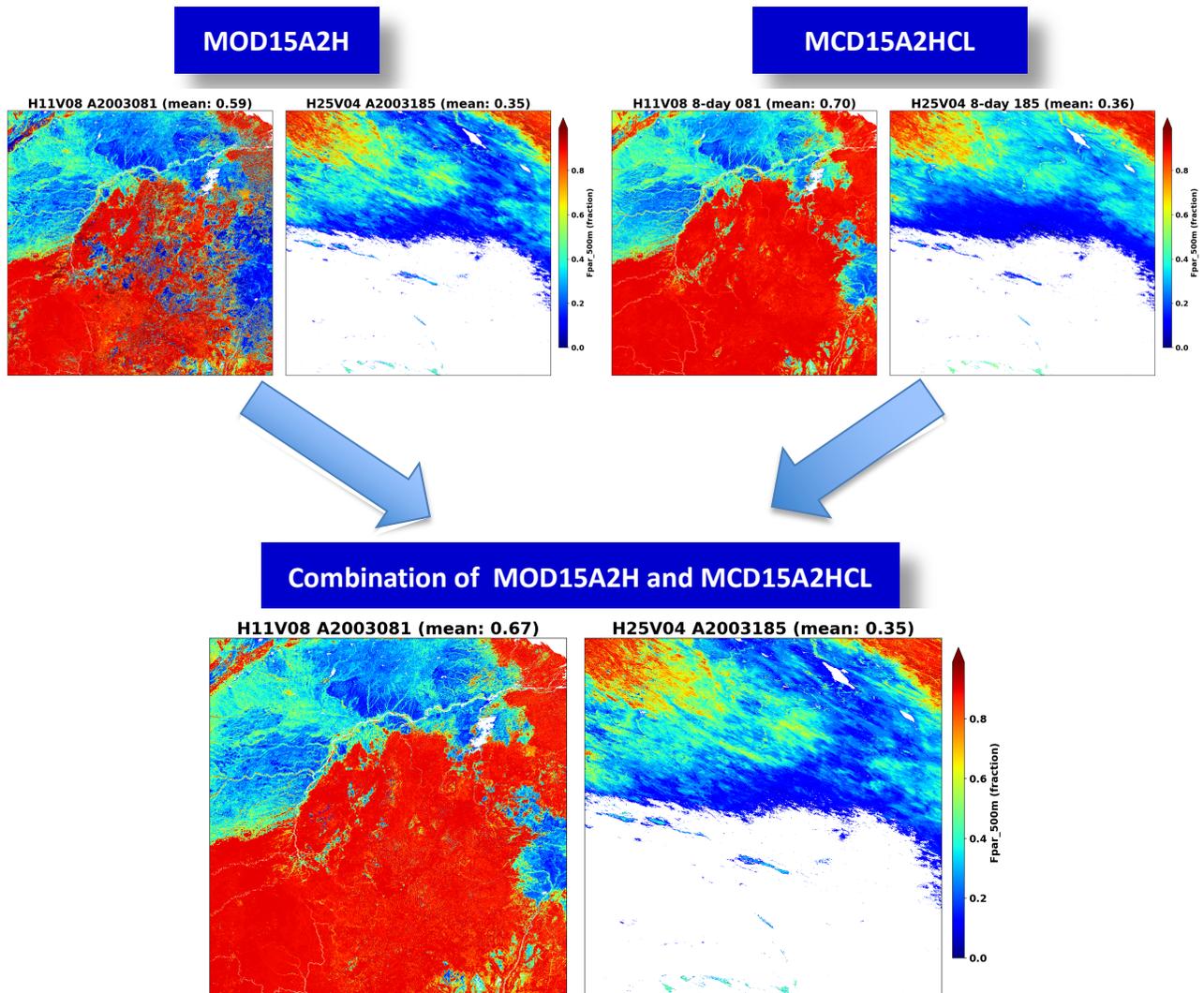
*Figure 3.2. The diagram shows how FPAR from MOD15A2H and MCD15A2HCL are combined to fill the gaps of contaminated FPAR in MOD15A2H using backup FPAR from MCD15A2HCL to enhance the forward MOD16 for two tiles H11V08 (Amazon) and H25V04 (Mongolia). Compared to the original FPAR from MOD15A2H, the combined FPAR is enhanced more for H11V08 in cloudy Amazon than H25V04 in clear Mongolia.*
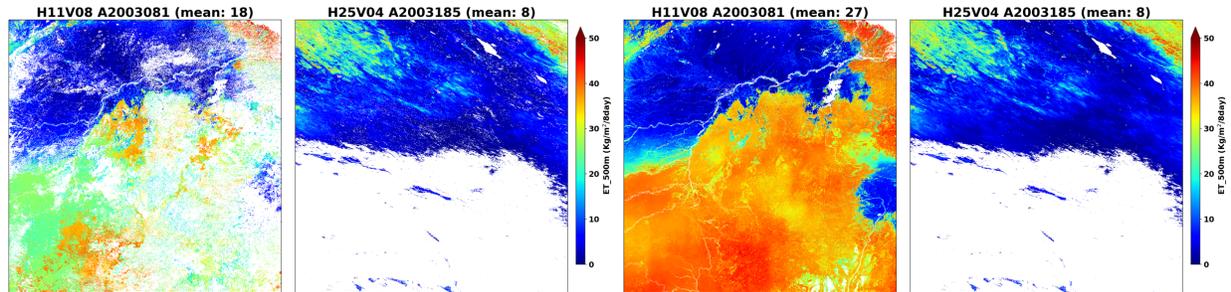
***Figure 3.3****. Comparison of ET from C6 MOD16A2 (left panel) with that from C6.1 (right panel) for two tiles of H11V08 (in Amazon) and H25V04 (in Mongolia). C6.1 now has much higher quality because data gaps caused by cloud contamination have been filled using climatology FPAR as input.*

Starting from C6.1 MOD16, we have introduced climatology FPAR/LAI and named it as MCD15A2HCL. The data from MCD15A2HCL are used as backup input to replace these contaminated FPAR/LAI from MOD15A2H for the corresponding 8-day periods. The 8-day MCD15A2HCL is the average of the best FPAR/LAI for a given vegetated pixel for the 8-day across the past 5 years based on the data quality from both MOD15A2H and MYD15A2H. If there is no reliable data available for an 8-day period across all 5 years, a temporally filling will be conducted to fill the gaps in climatology FPAR/LAI by following the gap-filling method proposed by Zhao et al. (2005). We chose 5-year because the time span for an interannual global scale climate fluctuation cycle, the El Niño-Southern Oscillation (ENSO), is about 5 years, and ENSO has great impacts on biosphere activities (Keeling et al., 1995; Nemani et al., 2003). A longer time span beyond 5-year may result in unrealistic climatology FPAR/LAI because averaging obscures vegetation greenness changes by ecosystem disturbances or land use cover change (Mildrexler et al., 2009; Song et al. 2018).

Figure 3.2 shows how the MOD16 process combines 8-day MOD15A2H with the corresponding 8-day climatology MCD15A2HCL to fill the gaps of contaminated FPAR/LAI for ET calculations. For a given pixel, if FPAR/LAI from MOD15A2H are contaminated, the corresponding climatology FPAR/LAI will be used to replace the contaminated values for calculations of ET, resulting in enhanced results. We use two tiles: H11V08 (in Amazon) and H25V04 (in Mongolia), as examples in the figures 2.2 and 2.3. Figure 2.2 shows that the combination of MOD15A2H and MCD15A2HCL results in a higher FPAR for H11V08, but almost no change of FPAR for H25V04. This is because Amazon region has high frequency of cloudiness whereas Mongolia in dry climate is clear most of time. MODIS albedo from the MODIS Terra/Aqua Combined Albedo product (MCD43) is another input required for MOD16 processing. Similar to the FPAR/LAI impact, C61 reprocessing of ET uses gap-filled MODIS albedo (Sun et al., 2017) for both year-end processing of MOD16GF and as backup to the operational Albedo product used as input in the processing of the operational standard MOD16A2 product in the forward processing.

Figure 3.3 shows the comparison of C6 and C6.1 MOD16A2H for two tiles H11V08 and H25V04 in Mongolia. Because C6 uses a fill value to for ET at a vegetated pixel when the input FPAR/LAI are contaminated, this caused that many pixels are invalid and show as data gaps in the cloudy Amazon tile H11V08. C6.1 solve this issue in C6 to use climatology MCD15A2HCL to

fill these gaps with bad quality FPAR/LAI, resulting in a "full" high quality MOD16A2H data products.  As expected, ET for tile H25V04 in Mongolia doesn't have much improvements because almost all FPAR/LAI have high quality in the region with a dry climate.

**|3.2.1.2. C6.1 MOD16A2[3] and Year-end Gap-filled MOD16A2[3]GF**

The C6.1 gap-filled MOD16 has different data product names and "GF" has been added to the names of the data files, such as M*D16A2GF and M*D16A3GF, to distinguish from the non-gap-filled M*D16A2 and M*D16A3.

The MOD16A2GF and MOD16A3GF will be generated at the end of each year when the entire yearly 8-day M*D15A2 are available, following the proposed method for improving MOD17 (Zhao et al., 2005).  Hence the gap-filled MOD16A2GF and MOD16A3GF are the improved MOD16 which have cleaned the contaminated inputs from 8-day FPAR/LAI. However, users cannot get MOD16A2[3]GF in the near real-time manner because it will be generated at the end of a given year. This is the limitation of the year-end gap-filling method.

Users should maintain caution, while using these Gap-filled products from the first years of the missions, 2000 and 2002 for MODIS TERRA and AQUA respectively. This is because, the temporal gap-filling algorithm, used to produce gap-filled FPAR/LAI inputs, could not have the full 8-days data in a year for ideally gap-filling, when it came to year 2000 for TERRA and 2002 for AQUA. MOD15A2H of TERRA starts from 2000-02-28 and MYD15A2H of Aqua from 2002-07-04.  Subsequently, the RANGEBEGINNINGDATE metadata value in M*D16A3GF for these first data years is consistent with the start date of M*D15A2H not from 200X-01-01.  Despite the RANGEBEGINNINGDATE metadata reflecting the start-of-mission date for TERRA (2000-02-28) and AQUA (2002-07-04) in M*D16A3GF for years 2000 and 2002, respectively, the Gap-filled FPAR/LAI inputs were processed using a temporal gap-filling over the entire year, with missing values from the start of the year till mission start.  The first available good FPAR/LAI from the start-of-mission date onward will be used for the missing values.

Therefore, users should especially be aware of using MYD16A2GF and MYD16A3GF in 2002, when the gap from the beginning of the year to actual start of mission (2002-07-04) is too long (> 0.5 year) and hence, the gap-filled FPAR/LAI inputs have no temporal dynamics for a vegetated pixel before 2002-07-04. As a result, the 8-day MYD16A2GF and the annual MYD16A3GF are less useful for 2002. The problem is similar for MOD16A2GF and MOD16A3GF in year 2000 but much less severe because there are just about 1.5 months data gap between start of the year and actual start of mission for Gap-filled versions of MOD15.

The detailed year-end gap-filling method is described in below section.

**3.2.1.3. Gap-filling FPAR/LAI for Year-end Gap-filled MOD16A2[3]GF**

At the end of each year, we solved the issue of the contaminated FPAR/LAI inputs to MOD16A2[3]GF by removing poor quality FPAR and LAI data based on the QC label for every pixel. If any LAI/FPAR pixel did not meet the quality screening criteria, its value is determined through linear interpolation between the previous period's value and that of the next period to pass the screening process (Zhao et a., 2005; Mu et al., 2007).  For any vegetated pixels, gap-filled or the improved MO[Y]D15A2H time series lead to improvements of MO[Y]D16. Under most conditions, 8-day composited ET will increase because the temporal filling process generally acts to increase FPAR and LAI, implying more vegetation cover and more leaves based on the logic of the MOD16 algorithm.

To further demonstrate how year-end gap-filling method improves the data quality, we chose two tiles: 1) h11v08 (left) in Amazon with frequent cloudiness (major land cover type is evergreen broadleaf forests) and 2) h25v04 (right) in Mongolia (major land cover types are grassland and barren) with high frequent clear sky. The two tiles representing the two extreme cases can reveal the improvements in the gap-filled MOD15A2H. For MOD15A2H, we just show FPAR because LAI has similar pattern to FPAR. For MO[Y]D16, we just show ET because changes of LE, PET and PLE have similar spatial pattern to ET.
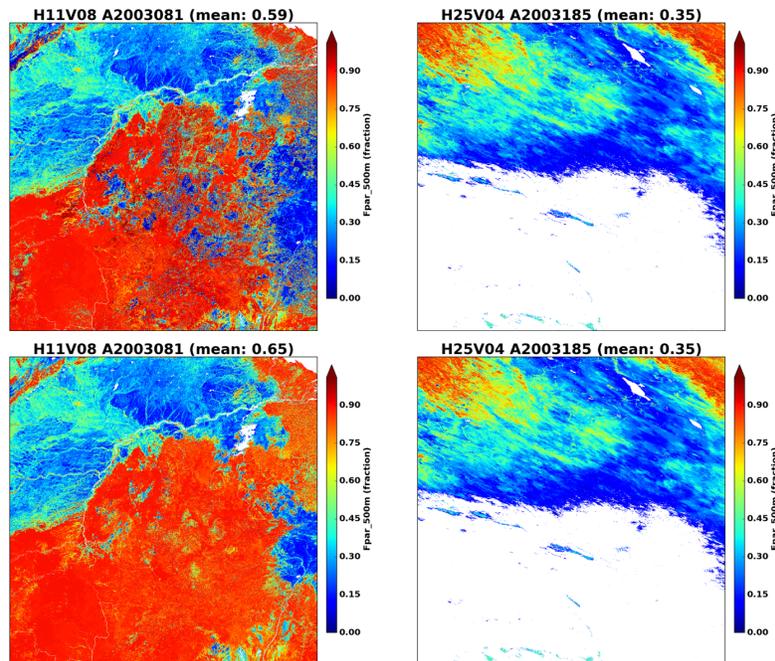


***Figure 3.4.*** *Comparisons of 8-day MOD15A2H FPAR from the original data (upper panel) with the year-end gap-filled (bottom panel) for two tiles. Cloudy area such as H11V08 in Amazon will be improved more than clear area H25V04 in Mongolia.*
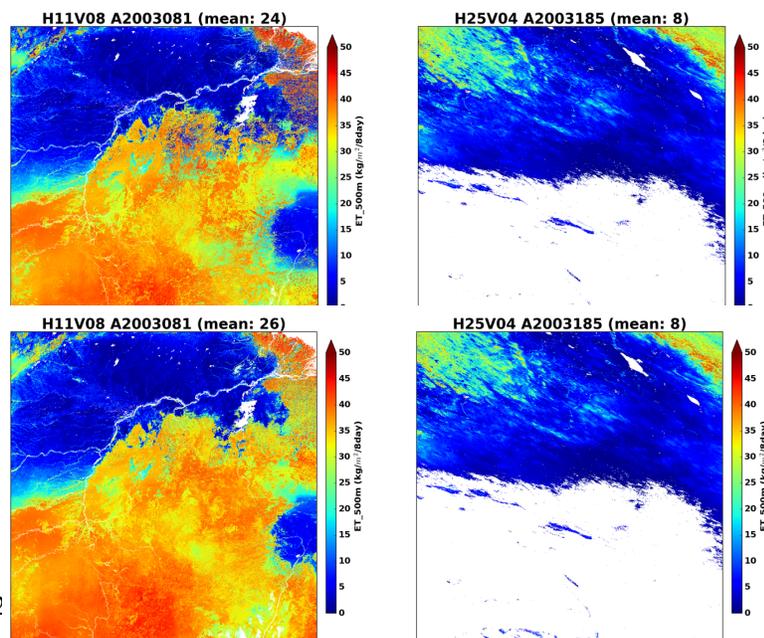
**Figure 3.5.** *Comparisons of 8-day MOD16A2 ET from the original data (upper panel) with the year-end gap-filled (bottom panel) for two tiles. Cloudy area such as H11V08 in Amazon will be improved more than clear area H25V04 in Mongolia.*
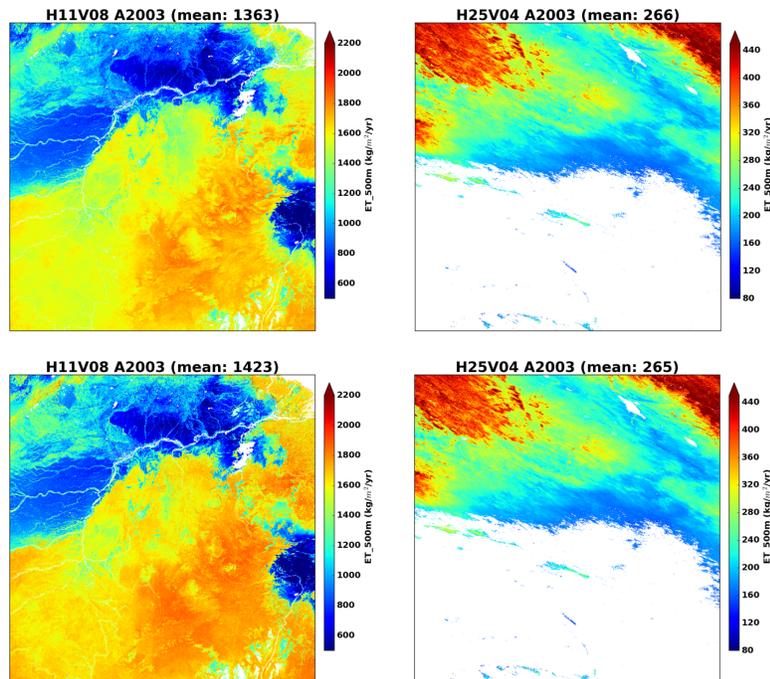


**Figure 3.6.** *Comparisons of the annual MOD16A3 ET from the original data (upper panel) with the year-end gap-filled (bottom panel) for two tiles. At the end of each year, MOD16A3GF will be generated using the year-end gap-filled MOD15A2H as input.*

## 3.3. GMAO daily meteorological data

The MOD16 algorithm computes ET at a daily time step. This is made possible by the daily meteorological data, including average and minimum air temperature, incident PAR and specific humidity, provided by NASA's Global Modeling and Assimilation Office (GMAO or MERRA GMAO), a branch of NASA (Schubert et al. 1993). These data, produced every six hours, are derived using a global circulation model (GCM), which incorporates both ground and satellite-based observations. These data are distributed at a resolution of 0.5° x 0.6° (MERRA GMAO) or 1.00° x 1.25° (*note that resolution may become finer with updates of GMAO system at NASA*) in contrast to the 0.5 km gridded MOD16 outputs. It is assumed that the coarse resolution meteorological data provide an accurate depiction of ground conditions and are homogeneous within the spatial extent of each cell.

One major problem is the inconsistency in spatial resolution between half-degree GMAO/NASA meteorological data and 0.5 km MODIS pixel. We solved the problem by spatially smoothing meteorological data to 0.5 km MODIS pixel level. For the problem arising from coarse spatial resolution daily GMAO data, we use spatial interpolation to enhance meteorological inputs. The four GMAO cells nearest to a given 0.5 km MODIS pixel are used in the interpolation algorithm. There are two reasons for choosing four GMAO cells per 0.5 km MODIS pixel: (1) this will not slow down the computational efficiency of creating MOD16, which is a global product, and (2) it is more reasonable to assume no elevation variation within four GMAO cells than more GMAO cells.

Although there are many formulae for non-linear spatial interpolation, for simplicity, we use a cosine function because the output value can be constrained between 0 and 1. This function still could not effectively boundary lines in a MOD16 image, and thus we utilized a modified cosine function of the form:

$$D_i = \cos^4((\pi/2)(d_i/d_{max})) \qquad i = 1,2,3,4$$
(23)

where, $D_i$ is the non-linear distance between the 0.5 km MODIS pixel and any one of four surrounding GMAO cells; $d_i$ is the great-circle distance between the 0.5 km pixel and the same GMAO cell; and $d_{max}$ is the great-circle distance between the two farthest GMAO cells of the four being used. This ensures that $D_i = 1$ when $d_i = 0$, and $D_i = 0$ when $d_i = d_{max}$.

Based on the non-linear distance ($D_i$), the weighted value $W_i$ can be expressed as

$$W_i = D_i / \sum_{i=1}^{4} D_i, \tag{24}$$

and therefore, for a given pixel, the corresponding smoothed value $V$ (i.e., interpolated Tmin, Tavg, VPD, SWrad) is

$$V = \sum_{i=1}^{4} (W_i V_i) \tag{25}$$

Theoretically, this GMAO spatial interpolation can improve the accuracy of meteorological data for each 0.5 km pixel because it is unrealistic for meteorological data to abruptly change from one side of GMAO boundary to the other. To explore the above question, we use observed daily weather data from World Meteorological Organization (WMO) daily surface observation network (>5000 stations) to compare changes in Root Mean Squared Error (RMSE) and Correlation (COR) between the original and enhanced DAO data. As a result of the smoothing process, on average, RMSE is reduced and COR increased for 72.9% and 84% of the WMO stations, respectively, when comparing original and enhanced DAO data to WMO observations for 2001 and 2002. Clearly, the nonlinear spatial interpolation significantly improves GMAO inputs for most stations, although for a few stations, interpolated GMAO accuracy may be reduced due to the inaccuracy of GMAO in these regions. (Zhao et al. 2005, 2006)

# 4. Validation of MOD16

To validate the MOD16 algorithm, we used the observed latent heat flux for 46 field-based eddy covariance flux towers, global 232 watersheds, as well as global results over the past 11 years (2000 to 2010). We cut out the input MODIS data for the 3 x 3 1-km$^2$ pixels surrounding each tower. We drove the MOD16 ET algorithm with both tower observed meteorological data and global GMAO meteorological data. We got the average ET estimates over those of the 3 x 3 1-km$^2$ pixels where the tower actual vegetation type is the same as MODIS land cover. Then we compared the ET estimates with the tower ET observations. For each of the seven biome types among the 46 flux towers except for CSH and OSH since there is only one tower with fewer than 365 measurements for each of them, we chose one tower to show the performance of MOD16 ET algorithm (Fig. 4.1).
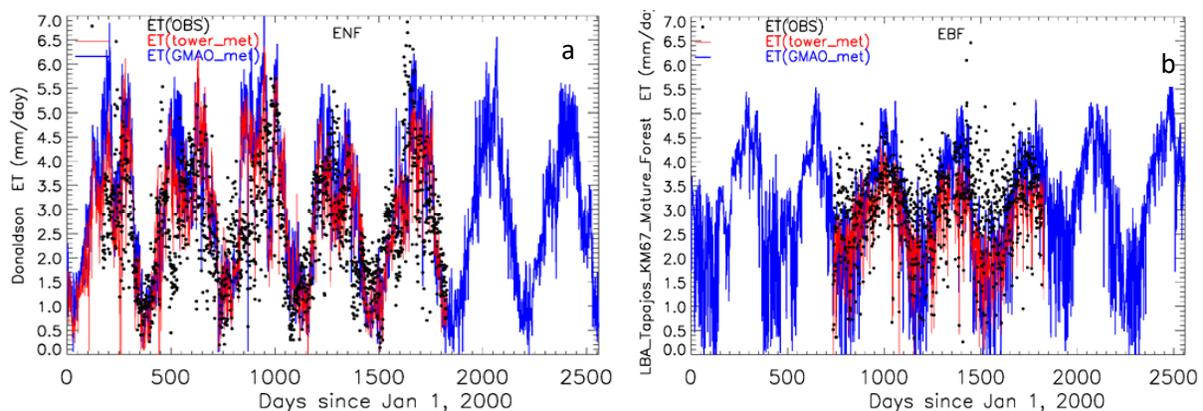


***Figure 4.1***. The ET measurements (black dots, OBS), the ET estimates driven by flux tower measured meteorological data (red lines) and GMAO meteorological data (blue lines) over 2000-2006 at seven tower sites, Donaldson (a) and LBA Tapajos KM67 Mature Forest (b).

The average daily ET biases between ET observations and ET estimates across the 46 towers are -0.11 kg/m$^2$/day driven by tower meteorological data and -0.02 kg/m$^2$/day driven by GMAO meteorological data. The average mean absolute errors (MAE) are 0.33 kg/m$^2$/day (tower-specific meteorology) and 0.31 kg/m$^2$/day (GMAO meteorology). The MAE values are 24.6% and 24.1% of the ET measurements, within the 10-30% range of the accuracy of ET observations (Courault et al. 2005; Jiang et al. 2004; Kalma et al. 2008).

# 5. Practical Details for downloading MOD16 Data

All MODIS land data products are distributed to global users from the USGS Land Processes Distributed Active Archive Center (USGS LP DAAC), found here:

https://lpdaac.usgs.gov/

Users are encouraged to explore the method to order and download data at the LDDAAC site above. A quick way to check MOD16 data and all other MODIS data is through USGS data pool site:

https://lpdaac.usgs.gov/tools/data-pool/

# 6. MOD16 Data Description and Process

## 6.1. Description and Process of MOD16 Data Files

There are two major MOD16 data sets, 8-day composite MOD16A2 and annual composite MOD16A3. Both MOD16A2 and MOD16A3 are stored in HDFEOS2 scientific data file format (http://hdfeos.org/software/library.php). HDFEOS2 file format is an extension of HDF4 by adding geo-reference, map projection, and other key meta data information to HDF4 format (https://support.hdfgroup.org/products/hdf4/) to facilitate users to use satellite data products from NASA's Earth Observing System (EOS) projects. Since MOD16 is a level 4 EOS data product, the grid data sets are saved in Sinusoidal (SIN) map projection, an equal-area map projection, with an earth radius of 6371007.181 meters (Note the inversed lat/lon are in WGS84 datum). The MODIS high-level data sets divide the global SIN into many chunks, so-called 10-degree tiles (https://modis-land.gsfc.nasa.gov/MODLAND_grid.html). There are 317 land tiles, and among which, 300 tiles (286 tiles for the Collection5) located within latitude of 60°S and 90°N (90°N for the Collection5) have vegetated land pixels. Therefore, for each 8-day Collection6 MOD16A2 and yearly MOD16A3, there are 300 land tiles globally if there are no missing tiles.

When MODIS updates MOD16 from the Collection5 to Collection6, the spatial resolution has increased from nominal 1-km (926.62543313883 meters) to 500m (463.312716569415 meters), to be consistent with changes in the spatial resolution of a major input to MOD16, the 8-day MOD15A2H.

For users don't know how to handle and process MODIS high-level data products, we suggest users to explore the method provided by USGS LPDAAC because their statement said that "*MRT has since been retired. Users are encouraged to use NASA Earthdata Search or AppEEARS. as an alternative to MRT*" (https://lpdaac.usgs.gov/news/modis-reprojection-tool-version-33-available/), or other tools such as HDF-EOS to GeoTIFF Conversion Tool (HEG) (http://hdfeos.org/software/heg.php ), or MODIS toolbox in ArcMap (https://blogs.esri.com/esri/arcgis/2011/03/21/global-evapotranspiration-data-accessible-in-arcmap-thanks-to-modis-toolbox/) to handle MOD16.

## 6.2. Description of MOD16 Date Sets

### 6.2.1. MOD16A2 (or MOD16A2GF)

Table 6.1 lists science data sets in the 8-day MOD16A2 or MOD16A2GF. ET_500m and potential ET (PET), PET_500m, are the ***summation*** of 8-day total water loss through ET (0.1 kg/m$^2$/8day), whereas the associated latent heat fluxes and its potential, LE_500m and PLE_500m, are the ***average*** total energy over a unit area for a unit day during the composite 8-day period (10000 J/m$^2$/day). But be cautious that the last 8-day (MOD16A2.A20??361.*.hdf) of each year is ***not*** 8-day but either 5-day or 6-day depending on normal or leap year.

As listed in Table 6.1, for valid data (Valid_data with the valid range) of MOD16A2 (or MOD16A2GF), the real value (Real_value) of each data set (ET, LE, PET or PLE) in the corresponding units (kg/m$^2$/8d or J/m$^2$/d) can be calculated using the following equation,

Real_value = Valid_data * Scale_Factor                                              (26)

*Table 6.1.* *The detailed information on science data sets in MOD16A2 (or MOD16A2GF)*

| Data Sets | Meaning | Units | Date Type | Valid Range | Scale Factor |
|---|---|---|---|---|---|
| ET_500m | 8-day total ET | kg/m$^2$/8d | int16 | -32767 ~ 32700 | 0.1 |
| LE_500m | 8-day average LE | J/m$^2$/d | int16 | -32767 ~ 32700 | 10000 |
| PET_500m | 8-day total PET | kg/m$^2$/8d | int16 | -32767 ~ 32700 | 0.1 |
| PLE_500m | 8-day average PLE | J/m$^2$/d | int16 | -32767 ~ 32700 | 10000 |
| ET_QC_500m | Quality Control | none | uint8 | 0 ~ 254 | none |

All data sets in MOD16A2 (or MOD16A2GF), except Quality Control (QC) data field, ET_QC_500m, have valid value ranging from -32767 to 32700 and are saved in signed 2-byte short integer (int16). Though data attributes list just one _FillValue: 32767 in the head file of MOD16A2 (or MOD16A2GF) file, there are, in fact, 7 fill values listed below for non-vegetated pixels, which we didn't calculate ET.

32767 = _Fillvalue
32766 = land cover assigned as perennial salt or Water bodies
32765 = land cover assigned as barren, sparse veg (rock, tundra, desert) (A2/A2GF), also used
                for data gaps from cloud cover and snow for vegetated pixels (A2)

32764 = land cover assigned as perennial snow, ice.
32763 = land cover assigned as "permanent" wetlands/inundated marshland
32762 = land cover assigned as urban/built-up
32761 = land cover assigned as "unclassified" or (not able to determine)

The QC data layer, ET_QC_500m, directly inherits the QC data field, Paralic, from the corresponding MOD15A2 of the same 8-day. Detailed information of bitfields in 8 bit word is the same as that from MOD15A2, as detailed below.

Data Field Name: ET_QC_500m

 BITS BITFIELD
 -------------
    0,0  MODLAND_QC bits

'0' =  Good Quality (main algorithm with or without saturation)
'1' =  Other Quality (back-up algorithm or fill values)


1,1 SENSOR
    '0' = Terra
    '1' = Aquí


2,2 DEADDETECTOR
    '0' = Detectors apparently fine for up to 50% of channels 1,2
    '1' = Dead detectors caused >50% adjacent detector retrieval


3,4  CLOUDSTATE (this inherited from Aggregate bits {0,1} cloud state)
    '00' = 0 Significant clouds NOT present (clear)
    '01' = 1 Significant clouds WERE present
    '10' = 2 Mixed cloud present on pixel
    '11' = 3 Cloud state not defined,  assumed clear


5,7  SCF_QC (3-bit, (range '000'..100') 5 level Confidence Quality score.
    '000' = 0, Main (RT) method used, best result possible (no saturation)
    '001' = 1, Main (RT) method used with saturation. Good, very usable
    '010' = 2, Main (RT) method failed due to bad geometry, empirical algorithm used
    '011' = 3, Main (RT) method failed due to problems other than geometry, empirical algorithm
used
    '100' = 4, Pixel not produced at all, value could not be retrieved (possible reasons: bad L1B
data, unusable MOD09GA data)


For non-improved NASA's operational MOD16A2, we suggest users at least exclude cloud-contaminated cells.  For the improved and reprocessed MOD16A2, users may ignore QC data layer because cloud-contaminated LAI/FPAR gaps have been temporally filled before calculating ET (Mu e al., 2007, also see previous section 3.2.1 and following 6.3).  QC just denotes if filled LAI/FPAR were used as inputs.  Because current operational MOD16A2 didn't calculate ET when the input MODIS data are unreliable, users may also ignore QC data layers for the NASA's operational MOD16 but just use pixels with values within the valid range.

### 6.2.2. MOD16A3 (or MOD16A3GF)

Table 6.2 lists science data sets in annual MOD16A3 (or MOD16A3GF). ET_500m and PET_500m are the ***summation*** of total daily ET/PET through the year (0.1 kg/m$^2$/year) whereas LE and PLE are the corresponding ***average*** total latent energy over a unit area for a unit day (10000 J/m$^2$/day) through the year. LE_500m and PLE_500m have the same unit, data type (signed 2-byte short int16), valid range and fill values as those listed above for the 8-day MOD16A2; whereas annual ET_500m and PET_500m are saved in unsigned 2-byte short integer (uint16) with valid range from 0 to 65528.

Similar to MOD16A2 (or MOD16A2GF), as listed in Table 6.2, for valid data (Valid_data with the valid range) of MOD16A3 (or MOD16A3GF), the real value (Real_value) of each data

set (ET, LE, PET or PLE) in the corresponding units (kg/m$^2$/yr or J/m$^2$/d) can be calculated using the following equation,

$$Real\_value = Valid\_data * Scale\_Factor \quad\quad (27)$$

Though data attributes list one _FillValue: 65535 in the HDFEOS MOD16A3 (or MOD16A3GF) file, there are, in fact, 7 fill values as listed below for non-vegetated pixels without ET calculations.

    65535 = _Fillvalue
    65534 = land cover assigned as perennial salt or Water bodies
    65533 = land cover assigned as barren,sparse veg (rock, tundra, desert) (A3/A3GF),
          also used for data gaps from cloud cover and snow for vegetated pixels (A3)
    65532 = land cover assigned as perennial snow, ice.
    65531 = land cover assigned as "permanent" wetlands/inundated marshland
    65530 = land cover assigned as urban/built-up
    65529 = land cover assigned as "unclassified" or (not able to determine)

**Table 6.2.** *The detailed information on science data sets in MOD16A3 (or MOD16A3GF)*

| Data Sets | Meaning | Units | Date Type | Valid Range | Scale Factor |
|---|---|---|---|---|---|
| ET_500m | annual sum ET | kg/m$^2$/yr | uint16 | 0 ~ 65500 | 0.1 |
| LE_500m | annual average LE | J/m$^2$/d | int16 | 0 ~ 32700 | 10000 |
| PET_500m | annual sum PET | kg/m$^2$/yr | uint16 | 0 ~ 65500 | 0.1 |
| PLE_500m | annual average PLE | J/m$^2$/d | int16 | 0 ~ 32700 | 10000 |
| ET_QC_500m | Quality Assessment | Percent (%) | uint8 | 0 ~ 100 | none |

QC data field in annual MOD16A3GF, ET_QC_500m, is different from most MODIS QC data sets because it is not bitfields but a more meaningful QC assessment for annual composite values. We used the method proposed by Zhao et al. (2005) to define annual ET QC as

$$ET\_QC\_500m = 100.0 \ x \ NUg/Totalg \quad\quad (28)$$

where NUg is the number of days during growing season with filled MODIS 500m LAI inputs to MOD16 due to missing or unfavorable atmospheric contaminated MODIS LAI (hence FPAR) if improvement reprocess is employed. Totalg is total number of days in the growing season. The growing season is defined as all days with Tmin above the value where stomata close as in the BPLUT. For example, an ET_QC_500m value of 85 for a pixel implies that during the growing days, for 85 percent of days, Gap-filled input FPAR/LAI had to be used because of unfavorable atmospheric conditions. As is expected, more humid forested regions tend to have high ET_QC_500m, whereas dry regions with grasslands or shrubs tend to have low ET_QC_500m (Figure 6c in Zhao et al., 2005).

The data type of ET_QC_500m is unsigned 1-byte integer (uint8) with valid range from 0 to 100. For vegetated land pixels, if ET_QC_500m has no spatial variations, it will imply the MOD16A3 is the NASA's operational data product, but not the improved by reprocessing because

frequency of cloud contaminations varies with space.  Though data attributes list one _FillValue: 255 in the HDFEOS MOD16A3 (or MOD16A3GF) file, there are, in fact, 7 fill values as listed below for non-vegetated pixels.

     255 = _Fillvalue
     254 = land cover assigned as perennial salt or Water bodies
     253 = land cover assigned as barren,sparse veg (rock, tundra, desert) (A3/A3GF), also
            used for data gaps (A3)
          from cloud cover and snow for vegetated pixels
     252 = land cover assigned as perennial snow, ice.
     251 = land cover assigned as "permanent" wetlands/inundated marshland
     250 = land cover assigned as urban/built-up
     249 = land cover assigned as "unclassified" or not able to determine

**LIST OF NTSG AUTHORED/CO-AUTHORED PAPERS
USING MOD16 ET:  2007 – 2015
[all available at https://scholarworks.umt.edu/ntsg_pubs/]**

Chen, Y., J. Xia, S. Liang, J. Feng, J. B. Fisher, X. Li, X. Li et al. (2014) Comparison of satellite-based evapotranspiration models over terrestrial ecosystems in China. *Remote Sensing of Environment* 140 (2014): 279-293.

Cleugh, H. A., Leuning, R., Mu, Q., and Running, S. W. (2007). Regional evaporation estimates from flux tower and MODIS satellite data. *Remote Sensing of Environment*, *106*(3), 285-304.

Jovanovic, N., Mu, Q., Bugan, R. D., and Zhao, M. (2015). Dynamics of MODIS evapotranspiration in South Africa. *Water SA*, *41*(1), 79-90.

Jung, M., Reichstein, M., Ciais, P., Seneviratne, S. I., Sheffield, J., Goulden, M. L., ... and Dolman, A. J. (2010). Recent decline in the global land evapotranspiration trend due to limited moisture supply. *Nature*, *467*(7318), 951-954.

Mu, Q., Heinsch, F. A., Zhao, M., and Running, S. W. (2007). Development of a global evapotranspiration algorithm based on MODIS and global meteorology data. *Remote Sensing of Environment*, *111*(4), 519-536.

Mu, Q., Jones, L. A., Kimball, J. S., McDonald, K. C., and Running, S. W. (2009). Satellite assessment of land surface evapotranspiration for the pan-Arctic domain. *Water Resources Research*, *45*(9).

Mu, Q., Zhao, M., and Running, S. W. (2011). Improvements to a MODIS global terrestrial evapotranspiration algorithm. *Remote Sensing of Environment*, *115*(8), 1781-1800.

Mu, Q., Zhao, M., and Running, S. W. (2011). Evolution of hydrological and carbon cycles under a changing climate. *Hydrological Processes*, *25*(26), 4093-4102.

Mu, Q., Zhao, M., & Running, S. W. (2012). Remote Sensing and Modeling of Global Evapotranspiration. In *Multiscale Hydrologic Remote Sensing: Perspectives and Applications* (pp. 443-480), edited by Chang, N. B., Hong, Y., CRC Press.

Mu, Q., Zhao M., Kimball J. S., McDowell N., and Running S. W., (2013) A Remotely Sensed Global Terrestrial Drought Severity Index, *Bulletin of the American Meteorological Society*, 94: 83–98.

Renzullo, L. J., Barrett, D. J., Marks, A. S., Hill, M. J., Guerschman, J. P., Mu, Q., and Running, S. W. (2008). Multi-sensor model-data fusion for estimation of hydrologic and energy flux parameters. *Remote Sensing of Environment*, *112*(4), 1306-1319.

Ruhoff, A. L., Paz, A. R., Aragao, L. E. O. C., Mu, Q., Malhi, Y., Collischonn, W., ... and Running, S. W. (2013). Assessment of the MODIS global evapotranspiration algorithm using eddy covariance measurements and hydrological modelling in the Rio Grande basin. *Hydrological Sciences Journal*, *58*(8), 1658-1676.

Smettem, K. R., Waring, R. H., Callow, J. N., Wilson, M., and Mu, Q. (2013). Satellite-derived estimates of forest leaf area index in southwest Western Australia are not tightly coupled to interannual variations in rainfall: implications for groundwater decline in a drying climate. *Global Change Biology*, *19*(8), 2401-2412.

Wang, S., Pan, M., Mu, Q., Shi, X., Mao, J., Brümmer, C., ... and Black, T. A. (2015). Comparing Evapotranspiration from Eddy Covariance Measurements, Water Budgets, Remote Sensing, and Land Surface Models over Canada. *Journal of Hydrometeorology*, *16*(4), 1540-1560.

Yao, Y., Liang, S., Li, X., Hong, Y., Fisher, J. B., Zhang, N., ... and Jiang, B. (2014). Bayesian multimodel estimation of global terrestrial latent heat flux from eddy covariance, meteorological, and satellite observations. *Journal of Geophysical Research: Atmospheres*, *119*(8), 4521-4545.

Zhang, K., Kimball, J. S., Mu, Q., Jones, L. A., Goetz, S. J., and Running, S. W. (2009). Satellite based analysis of northern ET trends and associated changes in the regional water balance from 1983 to 2005. *Journal of Hydrology*, *379*(1), 92-110.

**REFERENCES**

Belward, A. S., Estes, J. E., and Kline, K. D. (1999). The IGBP-DIS global 1-km land-cover data set DISCover: A project overview. *Photogrammetric Engineering and Remote Sensing*, *65*(9), 1013-1020.

Bouchet, R. J. (1963). Evapotranspiration reelle, evapotranspiration potentielle, et production agricole. *Ann. agron*, *14*(5), 743-824.

Choudhury, B. J., & DiGirolamo, N. E. (1998). A biophysical process-based estimate of global land surface evaporation using satellite and ancillary data I. Model description and comparison with observations. *Journal of Hydrology*, 205(3-4), 164-185.

Choudhury, B. (2000). A Biophysical Process-Based Estimate of Global Land Surface Evaporation Using Satellite and Ancillary Data. In *Observing Land from Space: Science, Customers and Technology* (pp. 119-126). Springer Netherlands.

Cleugh, H. A., Leuning, R., Mu, Q., and Running, S. W. (2007). Regional evaporation estimates from flux tower and MODIS satellite data. *Remote Sensing of Environment*, *106*(3), 285-304.

Courault, D., Seguin, B., and Olioso, A. (2005). Review on estimation of evapotranspiration from remote sensing data: From empirical to numerical modeling approaches. *Irrigation and Drainage systems*, *19*(3-4), 223-249.

Dang, Q. L., Margolis, H. A., Coyea, M. R., Sy, M., and Collatz, G. J. (1997). Regulation of branch-level gas exchange of boreal trees: roles of shoot water potential and vapor pressure difference. *Tree Physiology*, *17*(8-9), 521-535.

Dawson, T. E., Burgess, S. S., Tu, K. P., Oliveira, R. S., Santiago, L. S., Fisher, J. B., ... and Ambrose, A. R. (2007). Nighttime transpiration in woody plants from contrasting ecosystems. *Tree Physiology*, *27*(4), 561-575.

Friedl, M. A., Sulla-Menashe, D., Tan, B., Schneider, A., Ramankutty, N., Sibley, A., and Huang, X. (2010). MODIS Collection 5 global land cover: Algorithm refinements and characterization of new datasets. *Remote Sensing of Environment*, *114*(1), 168-182.

Fisher, J. B., Tu, K. P., and Baldocchi, D. D. (2008). Global estimates of the land–atmosphere water flux based on monthly AVHRR and ISLSCP-II data, validated at 16 FLUXNET sites. *Remote Sensing of Environment*, *112*(3), 901-919.

Jarvis, P. G. (1976). The interpretation of the variations in leaf water potential and stomatal conductance found in canopies in the field. *Philosophical Transactions of the Royal Society of London B: Biological Sciences*,*273*(927), 593-610.

Jiang, L., Islam, S., and Carlson, T. N. (2004). Uncertainties in latent heat flux measurement and estimation: implications for using a simplified approach with remote sensing data. *Canadian Journal of Remote Sensing*, *30*(5), 769-787.

Jones, H. G. (1992). *Plants and microclimate: a quantitative approach to environmental plant physiology*. Cambridge university press.

Kalma, J. D., McVicar, T. R., and McCabe, M. F. (2008). Estimating land surface evaporation: A review of methods using remotely sensed surface temperature data. *Surveys in Geophysics*, *29*(4-5), 421-469.

Kawamitsu, Y., Yoda, S., and Agata, W. (1993). Humidity pretreatment affects the responses of stomata and CO2 assimilation to vapor pressure difference in C3 and C4 plants. *Plant and Cell Physiology*, *34*(1), 113-119.

Kelliher, F. M., Leuning, R., Raupach, M. R., and Schulze, E. D. (1995). Maximum conductances for evaporation from global vegetation types.*Agricultural and Forest Meteorology*, *73*(1), 1-16.

Keeling, C. D., Whorf, T. P., Wahlen, M., & Van der Plichtt, J. (1995). Interannual extremes in the rate of rise of atmospheric carbon dioxide since 1980. *Nature*, *375*(6533), 666-670.

Leuning, R. (1995). A critical appraisal of a combined stomatal-photosynthesis model for C3 plants. *Plant, Cell & Environment*, *18*(4), 339-355.

Los, S. O., Pollack, N. H., Parris, M. T., Collatz, G. J., Tucker, C. J., Sellers, P. J., ... and Dazlich, D. A. (2000). A global 9-yr biophysical land surface dataset from NOAA AVHRR data. *Journal of Hydrometeorology*,*1*(2), 183-199.

Marsden, B. J., Lieffers, V. J., and Zwiazek, J. J. (1996). The effect of humidity on photosynthesis and water relations of white spruce seedlings during the early establishment phase. *Canadian Journal of Forest Research*,*26*(6), 1015-1021.

Mildrexler, D. J., M. Zhao, F. A. Heinsch, S. W. Running (2007). A new satellite-based methodology for continental-scale disturbance detection. *Ecological Applications*, 17: 235-250.


Mildrexler, D. J., M. Zhao, S. W. Running (2009). Testing a MODIS Global Disturbance Index across North America. *Remote Sensing of Environment*, 113: 2103-2117.

Misson, L., Panek, J. A., and Goldstein, A. H. (2004). A comparison of three approaches to modeling leaf gas exchange in annually drought-stressed ponderosa pine forests. *Tree Physiology*, *24*(5), 529-541.

Monteith, J. L. (1965). Evaporation and environment. In *Symposia of the Society for Experimental Biology* (Vol. 19, p. 205).

Mu, Q., Heinsch, F. A., Zhao, M., and Running, S. W. (2007). Development of a global evapotranspiration algorithm based on MODIS and global meteorology data. *Remote Sensing of Environment*, *111*(4), 519-536.

Mu, Q., Zhao, M., and Running, S. W. (2011). Improvements to a MODIS global terrestrial evapotranspiration algorithm. *Remote Sensing of Environment*, *115*(8), 1781-1800.

Nemani, R. R., C. D. Keeling, H. Hashimoto, W. M. Jolly, S. C. Piper, C. J. Tucker, R. B. Myneni and S. W. Running, 2003. Climate-driven increases in global terrestrial net primary production from 1982 to 1999. *Science*, 300: 1560-1563.

Oren, R., Sperry, J. S., Katul, G. G., Pataki, D. E., Ewers, B. E., Phillips, N., and Schäfer, K. V. R. (1999). Survey and synthesis of intra-and interspecific variation in stomatal sensitivity to vapour pressure deficit.*Plant, Cell & Environment*, *22*(12), 1515-1526.

Running, S. W., Loveland, T. R., and Pierce, L. L. (1994). A vegetation classification logic based on remote sensing for use in global scale biogeochemical models. *Ambio, 23*, 77-81.

Running, S. W., Nemani, R. R., Heinsch, F. A., Zhao, M., Reeves, M., and Hashimoto, H. (2004). A continuous satellite-derived measure of global terrestrial primary production. *Bioscience*, *54*(6), 547-560.

Running, S. W., and Kimball, J. S. (2005). Satellite-Based Analysis of Ecological Controls for Land-Surface Evaporation Resistance. *Encyclopedia of hydrological sciences*.

Sandford, A. P., and Jarvis, P. G. (1986). Stomatal responses to humidity in selected conifers. *Tree Physiology*, *2*(1-2-3), 89-103.

Schubert, S. D., Rood, R. B., and Pfaendtner, J. (1993). An assimilated dataset for earth science applications. *Bulletin of the American meteorological Society*, *74*(12), 2331-2342.

Schulze, E. D., Kelliher, F. M., Korner, C., Lloyd, J., and Leuning, R. (1994). Relationships among maximum stomatal conductance, ecosystem surface conductance, carbon assimilation rate, and plant nitrogen nutrition: a global ecology scaling exercise. *Annual Review of Ecology and Systematics*, 629-660.

Shuttleworth, W. J., and Wallace, J. S. (1985). Evaporation from sparse crops-an energy combination theory. *Quarterly Journal of the Royal Meteorological Society*, *111*(469), 839-855.

Song, X. P., Hansen, M. C., Stehman, S. V., Potapov, P. V., Tyukavina, A., Vermote, E. F., & Townshend, J. R. (2018). Global land change from 1982 to 2016. *Nature*, 560(7720), 639-643.

Sulla-Menashe, D., Gray, J. M., Abercrombie, S. P., & Friedl, M. A. (2019). Hierarchical mapping of annual global land cover 2001 to present: The MODIS Collection 6 Land Cover product. *Remote Sensing of Environment*, 222, 183-194.

Sun, Q., Z. Wang, Z. Li, A. Erb, and C. L. B. Schaaf (2017). Evaluation of the global MODIS 30 arc-second spatially and temporally complete snow-free land surface albedo and reflectance anisotropy dataset. *Intl. Journal of Applied Earth Observation & Geoinformation,* 58, 36-49, doi:10.1016/j.jag.2017.01.011.

Thornton, P.E. (1998). Regional ecosystem simulation: combining surface- and satellite-based observations to study linkages between terrestrial energy and mass budgets. PhD. Dissertation, School of Forestry, *The University of Montana*, Missoula, MT., 280 pp.

Tuzet, A., Perrier, A., and Leuning, R. (2003). Stomatal control of photosynthesis and transpiration: Results from a soil–plant–atmosphere continuum model. *Plant, Cell and Environment*, *26*, 1097-1116.

van de Griend, A. A., and Owe, M. (1994). Bare soil surface resistance to evaporation by vapor diffusion under semiarid conditions. *Water Resources Research*, *30*, 181-188.

Wan, Z., Zhang, Y., Zhang, Q., and Li, Z. L. (2002). Validation of the land-surface temperature products retrieved from Terra Moderate Resolution Imaging Spectroradiometer data. *Remote sensing of Environment*, *83*(1), 163-180.

White, M. A., Thornton, P. E., Running, S. W., and Nemani, R. R. (2000). Parameterization and sensitivity analysis of the BIOME-BGC terrestrial ecosystem model: net primary production controls. *Earth interactions*, *4*(3), 1-85.

Xu, L., and Baldocchi, D. D. (2003). Seasonal trends in photosynthetic parameters and stomatal conductance of blue oak (Quercus douglasii) under prolonged summer drought and high temperature. *Tree Physiology*, *23*(13), 865-877.

Zhao, M., Heinsch, F. A., Nemani, R. R., and Running, S. W. (2005). Improvements of the MODIS terrestrial gross and net primary production global data set. *Remote Sensing of Environment*, *95*(2): 164–176.

Zhao, M., Running, S. W., and Nemani, R. R. (2006). Sensitivity of Moderate Resolution Imaging Spectroradiometer (MODIS) terrestrial primary production to the accuracy of meteorological reanalyses. *Journal of Geophysical Research*, *111, G01002*, doi:10.1029/2004JG000004